Understanding Air-Core Photonic-Bandgap Fibers: Analogy to Conventional Fibers

Michel J. F. Digonnet, Hyang Kyun Kim, *Member, IEEE*, Gordon S. Kino, and Shanhui Fan

***Abstract*—It is shown from basic principles that the core modes of an air-core photonic-bandgap fiber (PBF) exhibit similar qualitative and quantitative behavior as the linearly polarized (LP) modes of an equivalent conventional fiber whose step-index profile is entirely determined by the band edges of the PBF. This analogy leads to the concept of effective numerical aperture (NA), which is used to provide an intuitive interpretation of the qualitative behavior of PBF modes. By using this equivalence, several key properties, including the number of modes, their cutoff, effective index, size, and divergence, and the dependence of these quantities on the PBF core and cladding parameters, can be predicted approximately by simulating the LP modes of the equivalent step-index fiber using standard LP-mode simulators or well-known formula. Besides providing a convenient tool to model the modes of a PBF, this analogy gives new physical insight into the fundamental characteristics of these complex waveguides.**

***Index Terms*—Air-core photonic-bandgap fibers, conventional solid-core fiber, LP modes, numerical aperture, PBF.**

I. Introduction

OVER the past few years, there has been a surge of interest in air-core photonic-bandgap fibers (PBFs), partly because of their fundamental appeal as intriguing new optical waveguides, and partly because of their numerous projected applications. To date, experimental work has been comparatively limited due to the high cost of these fibers, and research activity has been mostly theoretical. The basic physics of PBFs is well understood by experts in the field, and many optical properties have been analyzed, including transmission, phase and group velocity dispersion, and surface modes [1]–[5]. However, theoretical models require lengthy and expensive runs on a supercomputer, and they fail to give an intuitive feel for the behavior of these fibers. We have recently developed a novel numerical method that makes it possible for the first time to simulate PBFs in mere minutes on a personal computer [6], so part of this argument will soon be moot, but the fact remains that there is a strong need for a simple physical model of light propagation in PBFs. Such a model would provide greater physical insight as well as a means to quickly predict the mode properties of PBFs. It will also help neophytes grasp the basics of a rather complex new type of waveguide.

Manuscript received January 28, 2005; revised July 22, 2005. This work was supported by Litton Systems, Inc., a wholly owned subsidiary of Northrop Grumman.

The authors are with the Edward L. Ginzton Laboratory, Stanford University, Stanford, CA 94305 USA (e-mail: silurian@stanford.edu; hkkim@stanford.edu; kino@stanford.edu; shanhui@stanford.edu).

Digital Object Identifier 10.1109/JLT.2005.859406

In this paper, by comparing air-core fibers to conventional solid-core fibers, we develop a simple model that makes a significant contribution in this direction. We demonstrate that in spite of the major differences between the guiding mechanisms of these two types of fibers, the analogy between them can be pushed surprisingly far. We start by showing that the basic dispersion properties of a PBF can be well explained qualitatively in terms of what we know of conventional fibers by defining an equivalent numerical aperture (NA) for the PBF. Much as in the case of solid-core microstructured fibers [7], this definition provides a useful parameter by which to gauge a number of basic fiber properties, such as mode divergence and spot size. This NA is a frequency-dependent quantity that depends only on the PBF bandgap, which means that all that is required to evaluate the NA is a simple calculation of the bandgap. This concept of NA leads to the definition of an equivalent step-index fiber with the same core radius and NA as the PBF. Using simulations, we proceed to demonstrate that a PBF and its equivalent step-index fiber have similar quantitative mode properties. Such fundamental characteristics as the number of core modes, their dispersion, cutoff frequencies, intensity profile, and divergence, as well as the dependence of these quantities on frequency, core radius, air-filling ratio, and cladding geometry, can all be quickly calculated using existing formulas or simulators for linearly polarized (LP) modes. This approximate interpretation provides a new approach to analyze the modes of PBFs both qualitatively and quantitatively by comparing them to well-understood conventional fibers.

Throughout this paper, unless otherwise specified, we illustrate our arguments with an exemplary silica PBF with a cladding made of a two-dimensional periodic array of circular air holes in a triangular pattern. The cladding holes have a radius $\rho = 0.47\Lambda$, where Λ is the lattice period. The core is created by introducing a larger circular air hole of radius R at the center of the fiber, as illustrated in Fig. 1 for a few core radii [5]. The core radius is varied throughout the paper, as cited. Comparable quantitative and qualitative results have been obtained with other PBF structures. All exact simulations of the mode properties of this family of fibers were carried out using a full-vectorial plane-wave expansion method [8] on the University of Michigan AMD Linux cluster of parallel Athlon 2000MP processors. We used a grid resolution of $\Lambda/16$ and a supercell size of $8\Lambda \times 8\Lambda$. These values provided a good compromise between speed and accuracy. For example, decreasing the grid size to $\Lambda/32$ or increasing the supercell size to $10\Lambda \times 10\Lambda$ increased the simulation time about fourfold, but it modified the predicted effective indices of the modes

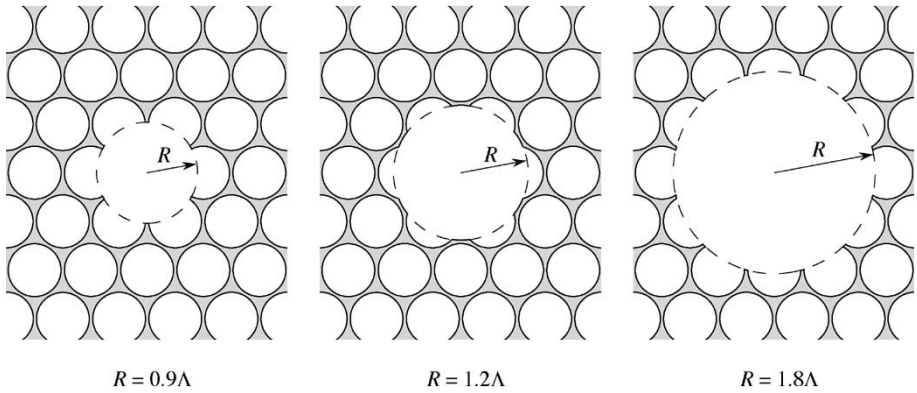

Fig. 1. Cross-sectional view of the air-core PBFs modeled in this work, shown for selected core radii R. The dashed circle is a construction curve that traces the circular core.

by less than 0.001. This change is essentially independent of wavelength, so it amounts only to a very slight and inconsequential shift in the dispersion curves. "Conventional fiber" refers to a traditional step-index fiber with a solid core and a solid cladding, in which guidance is provided by total internal reflection.

II. Concept of Equivalent Conventional Fiber

A. Numerical Aperture

To introduce the concept of equivalent conventional fiber in an air-core fiber, we refer to the dispersion diagram of Fig. 2(a), computed numerically for the exemplary fiber under study. Just like in a grating, the periodic structure in the fiber cladding introduces dead bands in the frequency space where modes cannot propagate along the fiber axis (z-direction). This region, shown as the shaded wedge in Fig. 2(a), is the bandgap. Adding a core introduces a defect in the photonic crystal that breaks its symmetry and allows a finite number of modes to propagate in the defect (core modes). We label $k_U(\omega)$ the wavenumber of the bandgap's upper edge at frequency ω, $k_L(\omega)$ the equivalent quantity for the lower edge, and $k_0(\omega) = \omega/c$ the light line, where c is the speed of light in vacuum. A pivotal frequency in this discussion is the frequency ω_0, where the light line crosses the lower band edge [$\omega_0 \approx 1.6733$ in units of $2\pi c/\Lambda$ in the example of Fig. 2(a)]. For a core mode to exist at ω, its propagation constant $k_z(\omega)$ must be both in the bandgap and below the light line, i.e., it must satisfy

$$k_U \leq k_z \leq k_L \tag{1a}$$

$$k_z \leq k_0. \tag{1b}$$

At frequencies above ω_0, $k_L > k_0$ [see Fig. 2(a)] and the two equations can be combined to give $k_U \leq k_z \leq k_0$. This inequality means that k_z can be equal to k_0. Since k_0 is the highest possible amplitude for a k vector in the core material (air), the implication is that the mode can propagate right along the fiber axis. The same argument can be made using the ray picture by considering the angle of propagation θ of the mode with respect to z. For a mode with a propagation constant k_z

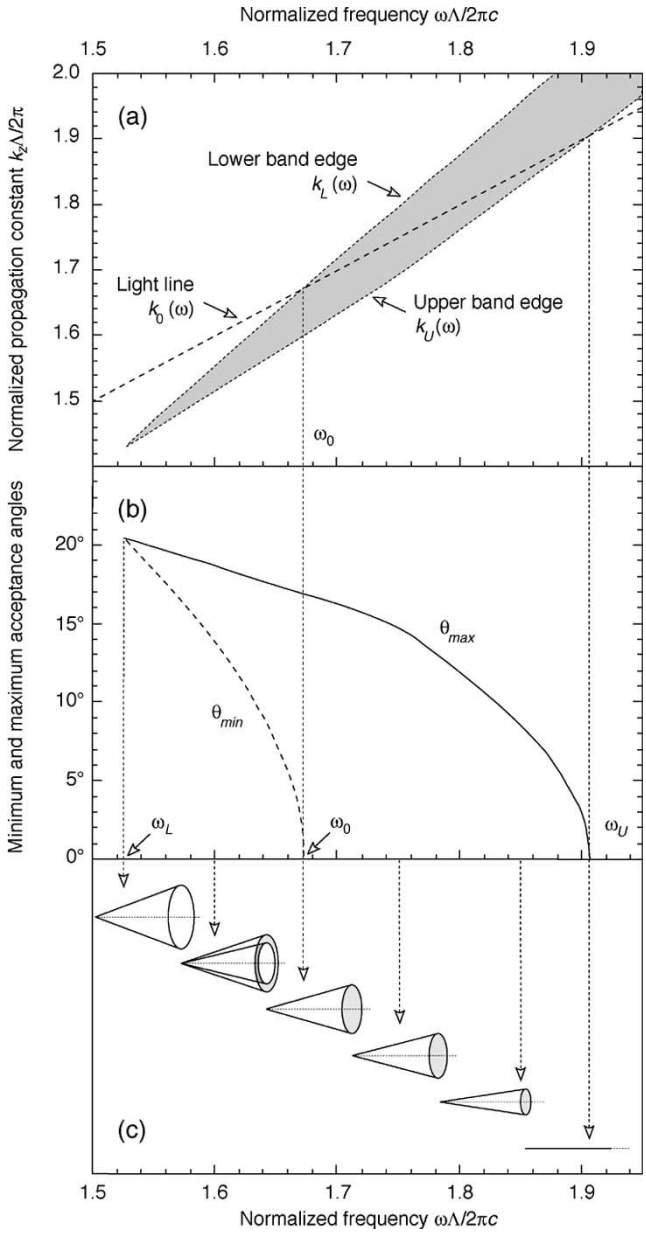

Fig. 2. (a) Calculated bandgap of the fiber under study. (b) Frequency dependence of the minimum and maximum acceptance angle of the fiber computed from (a). (c) Diagram of the fiber solid angle at representative frequencies.

traveling in a medium with a k-vector amplitude k_0, this angle is $k_z = k_0 \cos\theta$, or

$$\theta = \arccos\left(\frac{k_z}{k_0}\right). \tag{2}$$

When $k_z = k_0$, (2) yields $\theta = 0$, as expected. Similarly, the maximum possible propagation angle occurs when $k_z = k_U$ (the mode is then on the upper band edge). From (2), this angle is $\theta_{\max} = \arccos(k_U/k_0)$. Hence, the range of angles at which modes can propagate is $0 \le \theta \le \arccos(k_U/k_0)$. By analogy with a conventional fiber, we, therefore, define the NA of a PBF as $NA = \sin\theta_{\max}$, i.e.,

$$NA = \sin\left(\arccos\left(\frac{k_U}{k_0}\right)\right) = \sqrt{1-\left(\frac{k_U}{k_0}\right)^2} \qquad (\omega \ge \omega_0). \tag{3}$$

The acceptance region of the PBF is, thus, a solid cone, as in a conventional fiber. The main difference is that since k_U and k_0 are functions of ω, the NA and acceptance angle of a PBF are frequency dependent.

This analogy also enables us to define an equivalent refractive index for the core of a PBF and an equivalent refractive index for its cladding. In a step-index fiber with a core index n_1 and a cladding index n_2, the minimum value that k_z can take is $k_0 n_2$, and the maximum value is $k_0 n_1$. In an air-core PBF, this minimum value is k_U and the maximum value is k_0 [see (1)]. It follows that one can define the equivalent core and cladding indices of a PBF as

$$n_1 = 1 \tag{4a}$$

$$n_2 = \frac{k_U}{k_0} \tag{4b}$$

and we expect similarities between the mode behaviors of the PBF and of the equivalent step-index fiber with these two indices. This definition is, of course, entirely consistent with the definition of the NA: Inserting (4) in the traditional expression of the NA of a fiber $[NA = (n_1^2 - n_2^2)^{1/2}]$ yields (3).

For frequencies below ω_0, k_L is now smaller than k_0 [see Fig. 2(a)], so (1a) is sufficient. The range of propagation angles for core modes is now bounded by k_U and k_L, i.e., the minimum and maximum propagation angles are

$$\theta_{\min} = \arccos\left(\frac{k_L}{k_0}\right) \qquad (\omega \le \omega_0) \tag{5a}$$

$$\theta_{\max} = \arccos\left(\frac{k_U}{k_0}\right). \tag{5b}$$

The expression for $\theta_{\max}$ (5b) is the same as for $\omega \ge \omega_0$, but $\theta_{\min}$ is not: Since $k_L \le k_0$, $\theta_{\min}$ is no longer equal to zero, and now, *no mode can propagate right along the axis of the fiber*. There is a small cone of angles centered on the axis where the core does not guide optical power. In other words, the acceptance region of the PBF is a hollow cone. The fiber is now characterized by two NAs, namely 1) a minimum NA defined by the hollow portion of the cone and labeled NA' and 2) a maximum NA defined by the outer portion of the cone and labeled NA. From (5), these quantities are given by

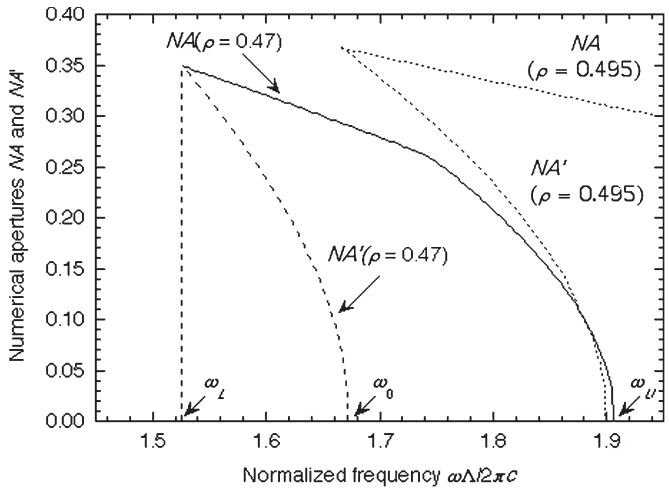

Fig. 3. Calculated frequency dependence of NA and NA' of the air-core PBF of Fig. 1 (solid and dotted curves, $\rho = 0.47\Lambda$), and of a PBF with the same geometry but a larger cladding hole radius ($\rho = 0.495\Lambda$, dotted curves).

$$NA' = \sin(\theta_{\min}) = \sqrt{1-\left(\frac{k_L}{k_0}\right)^2} \tag{6a}$$

$$NA = \sin(\theta_{\max}) = \sqrt{1-\left(\frac{k_U}{k_0}\right)^2}. \tag{6b}$$

As we shall see, NA is equivalent to the NA of a conventional solid-core fiber, while NA' is a new quantity that characterizes the low-angle "hole" in the acceptance region. Again, both NA and NA' are frequency dependent. It is important to note that (6a) also holds above ω_0: In that range, $k_L = k_0$ and (6a) yields $NA' = 0$, which is correct. Similarly, (6b) is identical to (3) and, therefore, it holds for $\omega \ge \omega_0$ as well. Therefore, (6a) and (6b) are valid at all frequencies within the bandgap.

The calculated frequency dependence of the propagation angles $\theta_{\min}$ and $\theta_{\max}$ and of the acceptance region are plotted in Fig. 2(b) and (c), respectively. The propagation angles were calculated simply by inserting the calculated frequency-dependent wavenumbers $k_U(\omega)$, $k_L(\omega)$, and $k_0(\omega)$ [see Fig. 2(a)] in (5). At the lowest bandgap frequency ω_L, $\theta_{\min} = \theta_{\max}$, the acceptance region vanishes, and no modes can propagate. As ω increases, $\theta_{\min}$ and $\theta_{\max}$ decrease, but $\theta_{\min}$ remains smaller than $\theta_{\max}$ and the core can support modes. The acceptance region is a hollow cone [see Fig. 2(c)]. As ω approaches ω_0, this cone becomes smaller ($\theta_{\max}$ decreases), and it gradually fills in ($\theta_{\min}$ decreases), until at ω_0, $\theta_{\min}$ reaches zero and the cone is full [see Fig. 2(c)]. Above ω_0, $\theta_{\min} = 0$ and $\theta_{\max}$ continue to drop [see Fig. 2(b)], i.e., the acceptance region is a solid cone of diminishing angle, until at the highest bandgap frequency ω_U, the cone vanishes [see Fig. 2(c)]. At ω_U and above, all core modes are cut off. The frequency dependencies of NA and NA', calculated from (6a) and (6b), are plotted in Fig. 3. From ω_L, where they are equal, NA and NA' are decreasing functions of frequency. NA' reaches zero at $\omega = \omega_0$ and stays at zero for $\omega \ge \omega_0$. The value of NA ranges from 0 to 0.35, i.e., it is of the same order as the NA of a conventional fiber.

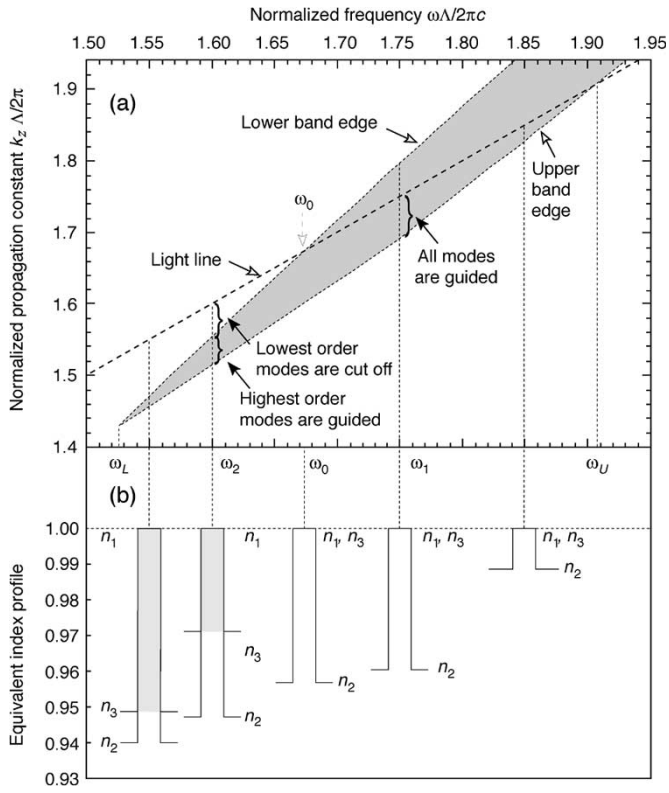

Fig. 4. (a) Bandgap diagram illustrating regions where lowest order modes are cut off (below ω_0, e.g., at ω_2) and guided (above ω_0, e.g., at ω_1). (b) Index profile of the equivalent conventional fiber at selected frequencies.

The existence of two NAs below ω_0 can be understood physically as follows. In this frequency range, the PBF can only support modes that propagate at large angles [see Fig. 2(b)], i.e., higher order modes but not lower order modes. The order of the highest order guided mode, and the properties of these modes, are by and large controlled by NA: For these modes, the PBF behaves approximately like a conventional fiber with an NA equal to NA. However, the lower order modes that would propagate mostly at angles smaller than $\theta_{\min}$ are not guided. Which low-order modes are cut off is dictated by NA'. This is illustrated graphically in Fig. 4(a), which reproduces the dispersion diagram of Fig. 2(a). At frequency ω_1 (above ω_0), the entire region below the light line lies in the bandgap, which means that all modes (lower and higher order) are guided. In contrast, at frequency ω_2 (below ω_0), the region between the light line and the lower band edge, which defines NA', is where lower order modes would propagate, but these modes cannot propagate, because they fall outside the bandgap. The order of the last low-order mode not guided by the PBF is set by NA'. The region between the band edges is where core modes are guided, but these are higher order modes [see Fig. 4(a)]. To summarize, NA' determines which low-order modes are not guided, and NA determines which high-order modes are guided. Note that the fact that the center of the cone does not support k vectors does affect the properties of the high-order modes guided by the fiber. However, this effect is weak, especially for modes far from cutoff, and the statement made above that the mode properties are largely controlled by NA is a good one, as demonstrated further on.

B. Equivalent Index Profile

In the light of these considerations, we can also define an equivalent index for the core and the cladding of a PBF for $\omega < \omega_0$. Since the main NA that controls the properties of core modes is NA (6b), the behavior of the PBF is expected to show similarities to the behavior of an equivalent conventional fiber with a core index $n_1 = 1$ and a cladding index $n_2 = k_U/k_0$. This definition is the same as in the $\omega < \omega_0$ region, i.e., (4) holds at all frequencies. Similarly, to account for the hollow portion of the acceptance region (quantified by NA'), we define a third index n_3 that controls the cutoff of low-order modes. From the expression of NA' (6a), this index is $n_3 = k_L/k_0$. To illustrate these important definitions, we show in Fig. 4(b) a schematic of the equivalent step-index profile of the air-core PBF at selected frequencies across the bandgap. As the frequency is increased from ω_L, the effective core index remains constant and equal to 1, while the effective cladding index n_2 monotonically increases towards 1, which it reaches at ω_U. The shaded portion in each index profile in the $\omega < \omega_0$ region represents NA': The modes whose effective indices fall within these shaded regions (index above n_3) are not guided.

It is important to appreciate that NA and NA' depend only on the location of the band edges in the $\omega - k$ plane. Since the bandgap of a PBF is very weakly affected by the presence of the core, NA and NA' are essentially independent of the core geometry and size. On the other hand, they depend on all the parameters that affect the band edges, such as the crystal symmetry and the cladding hole size. As an example, we show in Fig. 3 NA and NA' computed for the same triangular symmetry but for larger cladding air holes ($\rho = 0.495\Lambda$). Increasing the air-hole size opens the bandgap and moves it towards higher frequencies [9], which results in NAs that are larger and downshifted in frequency.

C. Equivalent V Number

With these definitions in place, we can define the equivalent normalized frequency of a PBF in the same way as for a conventional fiber, namely

$$V = \frac{2\pi R NA}{\lambda} \tag{7a}$$

where λ is the optical wavelength and R is the core radius. The portion of the fiber that does not guide light is characterized by a second V number

$$V' = \frac{2\pi R NA'}{\lambda}. \tag{7b}$$

Because NA and NA' are strongly decreasing functions of frequency, both V and V' monotonically *decrease* as the frequency increases, which is the opposite behavior of a conventional fiber. In a PBF, the V number scales up with wavelength, not with frequency.

In the rest of this paper, we use the NA concept and the equivalence to conventional fibers established in this section to compare key properties of the modes of an air-core PBF to the LP modes of its equivalent step-index fiber. We investigate

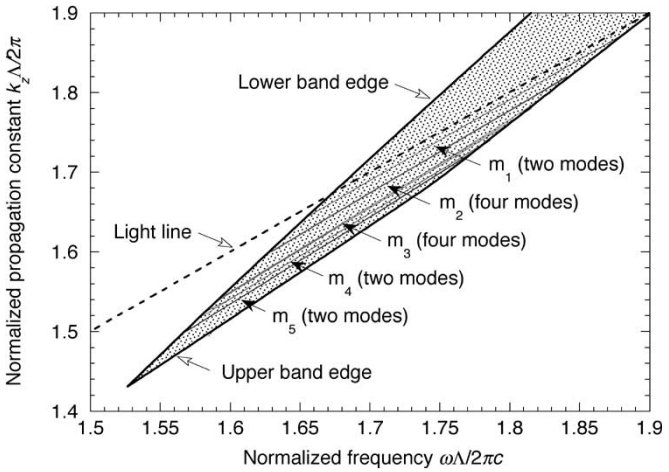

Fig. 5. Calculated dispersion curves of the core modes of the PBF of Fig. 1 for a core radius $R = 1.8\Lambda$.

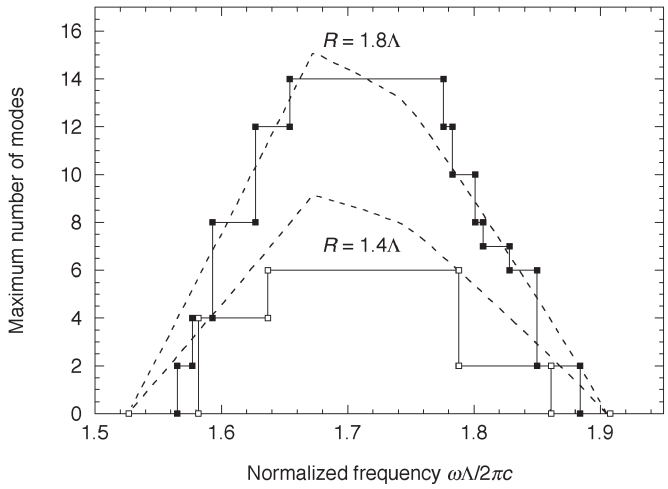

Fig. 6. Frequency dependence of the number of core modes calculated exactly for a core radius $R = 1.8\Lambda$ (solid squares) and $R = 1.4\Lambda$ (open squares). Dashed curves are the approximate predictions of the LPMA model.

in particular the accuracy of what we refer to as the LP mode approximation (LPMA) model, which approximates properties of PBF core modes by the properties of the LP modes of its equivalent step-index fiber.

III. Number of Modes Versus Frequency

Fig. 5 shows the calculated dispersion curves of all the core modes of the PBF under study for a core radius $R = 1.8\Lambda$. The first modes that appear at lower frequency are the highest order modes. Because of degeneracy, these modes occur in a group of degenerate modes, labeled m_5, with nearly identical dispersion curves. As the frequency increases, a second group of modes (m_4) appears, then a third (m_3), a fourth (m_2), and a fifth (m_1), the modes within each new group having a lower order than those of the previous group. As discussed elsewhere [10], based on their field symmetry, the composition of these groups is as follows: Group m_1 contains the two fundamental HE_{11} modes; group m_2 the next four higher order modes, labeled TM_{01}, HE_{21} odd and even, and TE_{01}; group m_3 (four modes) the odd and even EH_{11} modes and the odd and even HE_{31} modes; group m_4 (two modes) the odd and even HE_{12} modes; and, finally, group m_5 (two modes) the odd and even HE_{41} (or EH_{21}) modes. This mode distribution is the same as for a conventional fiber [11]. The number of modes is maximum in the vicinity of ω_0. As the frequency increases above ω_0, the groups disappear one by one in the order they appeared: Group m_5 disappears first, followed by m_4, m_3, and m_2, until only the fundamental modes remain. The fiber is "single mode" only at the highest frequencies, just before the light line crosses the upper band edge and they cut off, too.

This mode-count behavior is in sharp contrast with that of a conventional fiber, in which 1) the NA is independent of frequency, and, thus, the number of modes increases monotonically with increasing frequency, and 2) the modes have a low-frequency cutoff but no high-frequency cutoff. The different behavior of PBFs is very well explained by the physical arguments presented in Section II. At the lowest frequencies (ω just above ω_L), the PBF's acceptance region is a hollow cone that can only support the highest order modes. As the frequency is increased, the acceptance cone fills in [see Fig. 2(c)], and lower order mode groups gradually reach cutoff and become guided. At $\omega = \omega_0$, the "available" NA, $NA - NA'$, is maximum, and so is the number of guided modes. As the frequency increases above ω_0, the acceptance cone is solid, but it gets smaller, i.e., NA decreases, and the number of guided modes decreases like it does in a conventional fiber, i.e., the higher order modes go first. This qualitative agreement with Fig. 5 fully supports our NA definitions.

To further test this analogy between PBFs and conventional fibers, we plot in Fig. 6 the dependence of the number of core modes on frequency for the same PBF (solid squares connected by segments, same data as Fig. 5). Again, the number of modes grows in steps from zero at ω_L to a maximum (14 in this case) around ω_0, then drops to zero at ω_U. From basic electromagnetic theory, it is well-known that for a conventional fiber, the number of core modes at ω is closely approximated by $N(\omega) \approx V^2/2$ [12]. In a PBF, $N(\omega)$ is equal to the number of modes guided by the equivalent step-index fiber numerical aperture (NA) minus the lower order modes that fall within the hollow cone numerical aperture (NA') and are, thus, not guided. Therefore

$$N(\omega) \approx \frac{V^2}{2} - \frac{V'^2}{2}. \tag{8}$$

This expression was first proposed by Cregan *et al.* [13] to estimate the minimum core radius that will support a mode. By inserting the expressions of V and V' (7) in (8), then replacing NA and NA' by their respective expression (6), we obtain the approximate expressions for the number of core modes in an air-core PBF

$$N(\omega) \approx \frac{1}{2}\left(\frac{2\pi R}{\lambda}\right)^2 \left[\left(\frac{k_L}{k_0}\right)^2 - \left(\frac{k_U}{k_0}\right)^2\right], \qquad \omega \le \omega_0$$

$$\approx \frac{1}{2}\left(\frac{2\pi R}{\lambda}\right)^2 \left[1 - \left(\frac{k_U}{k_0}\right)^2\right], \qquad \omega \ge \omega_0. \tag{9}$$

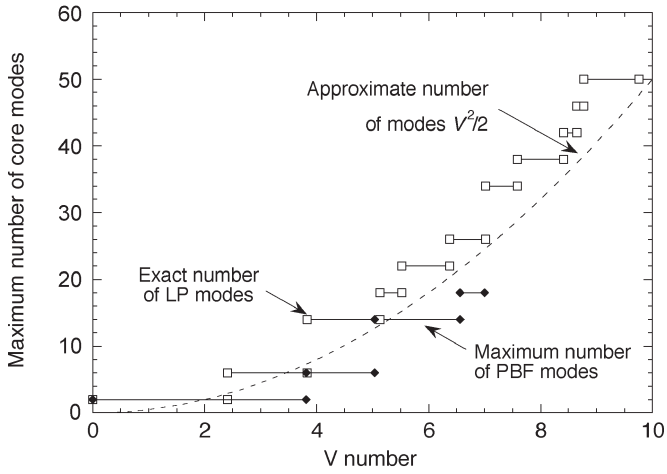

Fig. 7. Maximum number of modes supported by the air-core PBF of Fig. 1 as a function of the fiber V number, calculated using the exact MPB model (solid diamonds), the approximate LPMA model (open squares), and the approximate formula for LP modes (9) (dashed curve).

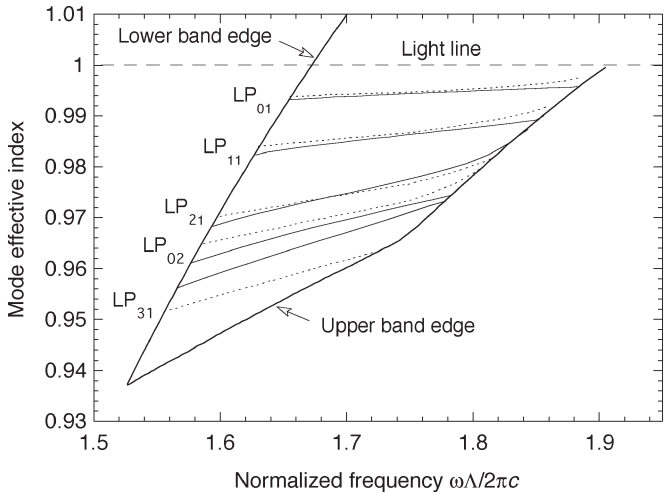

Fig. 8. Dispersion of the modes of a multimode air-core PBF ($R = 1.8\Lambda$), calculated with the exact model (solid curves) and with the LPMA model (dashed curves).

Again, the top expression is valid at all frequencies by replacing k_L by k_0 when $\omega > \omega_0$. Note that the maximum number of core modes (which occurs around ω_0) is given by (8) in which $V' = V'(\omega_0) = 0$, or $N(\omega) \approx V^2/2$: It is the same approximate formula as for a conventional fiber.

Applied to this fiber with $R = 1.8\Lambda$, (9) yields the top dotted curve in Fig. 6. The agreement with the exact dependence is reasonable, not only above ω_0, where the PBF's solid angle is filled and a PBF is expected to behave most closely like a conventional fiber, but also below ω_0, where the acceptance cone is hollow. The nonmonotonic behavior in the number of modes and the agreement with (9) apply for all core radii, as illustrated in Fig. 6 for $R = 1.4$ (lower two curves). The agreement improves for more highly multimoded fibers, as in conventional fibers.

Since the two fibers in Fig. 6 have the same cladding, the NA dependence on frequency used to generate the two approximate curves is the same. The two dashed curves differ only in their core radius R, which means that they are scaled differently [see (9)]: Their ratio is simply $(1.8/1.4)^2 \approx 1.65$ at all frequencies. This frequency dependence of the number of core modes is contained entirely in the bandgap, which is quick to compute. Calculating the approximate number of modes carried by a family of fibers with the same photonic-crystal cladding (and, thus, the same bandgap) but different core radii requires simulating this bandgap only once.

IV. Number of Modes Versus Core Radius

Fig. 7 plots the exact dependence of the maximum number of modes (N at $\omega \approx \omega_0$) supported by the PBF on the V number. It was generated by simulating the fiber dispersion for different core radii, counting the number of modes N for each R, and plotting N versus V. As the core radius increases, the number of modes increases in sudden steps from 0 to 2, then 6, 14, 18, etc. For comparison, Fig. 7 also shows this dependence for the LP modes of a weakly guiding step-index fiber. The behavior is quite similar. As V increases, the number of modes jumps up in incremental steps of generally four (the degeneracy of LP modes) every time V reaches the cutoff value of the next LP mode. Occasionally, the height of the jump is eight when two modes happen to have the same cutoff (accidental degeneracy). The number of modes, thus, evolves from 2 to 6, then 14, 18, 22, 26, 34, etc. The sequence is the same in a PBF. The main difference is that in a PBF the cutoffs are shifted to higher V numbers. Note that the exact curve in Fig. 7 (solid diamonds) is not a universal curve: The cutoff V values only apply at ω_0, and they are affected by the PBF geometry and the air-filling ratio. For the fiber simulated here, the upper cutoff for the fundamental modes is $V = 3.816$ (compared to ~ 2.405 for a conventional fiber). The dashed curve in Fig. 7 represents the approximate number of LP modes predicted by (9) at ω_0. The prediction of the LPMA model is as good for the PBF as it is for a conventional fiber. These results confirm that (9) constitutes a good approximation of the number of modes of a PBF.

V. Cutoff Frequencies of Individual Modes

Fig. 8 shows the exact simulated dispersion curves of the PBF modes for $R = 1.8\Lambda$. These curves are the same as in Fig. 5, except that to follow the conventional representation favored in fiber optics, they are plotted as the mode effective index $n_{\text{eff}} = k_z/k_0$ versus frequency. This figure also shows the band edges and the light line (a horizontal line of index 1 in this representation). For clarity, only one mode per group is represented. As in a conventional fiber, at a given frequency, the effective index is highest for the fundamental modes, and it decreases as the mode order increases. This description is analogous to the discrete energy levels of a potential well. Here, the maximum index (energy) is set by the light line (lowest possible phase velocity) and the minimum index by the lower band edge.

For each mode group, the low-frequency cutoff occurs at the crossing point of the dispersion curve with the lower band edge, and it is, thus, controlled by NA'. The high-frequency cutoff occurs at the crossing point with the upper band edge, and it

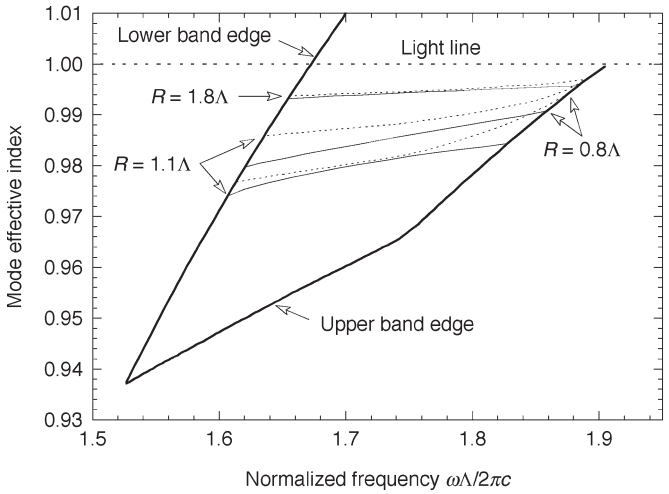

Fig. 9. Dispersion of the fundamental modes of the air-core PBF for three values of the core radius R, calculated with the exact model (solid curves) and with the LPMA model (dashed curves).

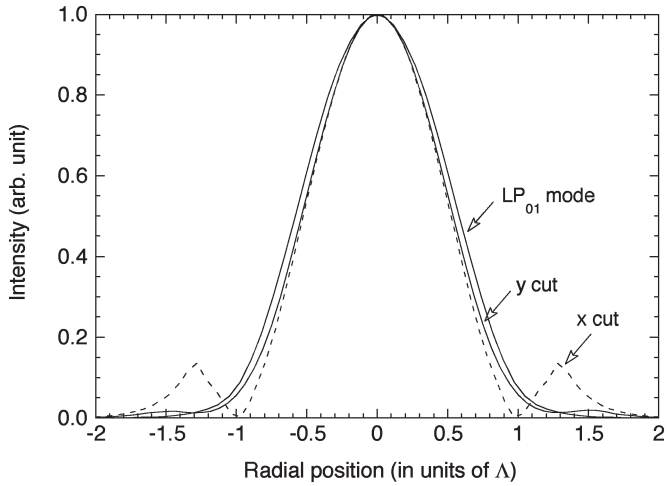

Fig. 10. Calculated x-cut and y-cut radial intensity profile of the fundamental mode of the air-core PBF at the normalized frequency of 1.6156 for a core radius $R = 0.9\Lambda$, and calculated profile of the LP_{01} mode of the equivalent conventional fiber.

is controlled by NA. Interestingly, the low-frequency cutoff of the fundamental modes is not far below ω_0 (see Fig. 8). The physical reason is that below ω_0, the acceptance region of the fiber is a hollow cone. Since the angular (Fourier) spectrum of the fundamental mode is essentially a Gaussian, much of the mode energy is confined to small angles, which the PBF cannot guide. That the cutoff is not exactly at ω_0 indicates that the mode can tolerate some low-angle filtering and still exist in a PBF with a slightly hollow acceptance cone, but this tolerance is expectedly limited and the mode cuts off not far below ω_0. In the example of Fig. 8, at this cutoff, $NA'/NA \approx 0.38$: The mode cuts off when the fraction of its angular spectrum that is no longer guided reaches $\sim 38\%$.

VI. Approximate Dispersion Curves

In the light of the equivalence between an air-core PBF and a step-index fiber, it was interesting to attempt predicting the dispersion curves of a PBF by simulating the LP modes of its equivalent conventional fiber (LPMA model). To do so, we used a standard LP-mode simulator to compute the dispersion curves of the guided modes of the PBF under study (Fig. 8; $R = 1.8\Lambda$), using as an input the frequency-dependent cladding index n_2. The result of this LPMA simulation is shown as the dotted curves in Fig. 8. There is good agreement between the approximate and exact dispersion curves for the three lowest mode groups at all frequencies, especially towards the center of the bandgap. For example, for the fundamental modes at the normalized frequency of 1.6710, the approximate n_{eff} is 0.99398, compared to the exact value of 0.99355 (mean of the two modes), or an error of only 0.04%. The agreement is not as good for higher order modes (LP_{02} and LP_{31}). The LPMA model certainly cannot be expected to predict higher order derivatives of the dispersion, such as group velocity, but it predicts the effective indices of lower order modes reasonably well. The accuracy of the LPMA model depends on the core radius, as illustrated in Fig. 9. The accuracy is fairly good for large cores (multimode fibers), but in single-mode fibers ($0.5\Lambda \leq R \leq 1.2\Lambda$ for this filling ratio), the LPMA model can only predict an approximate value for the effective index of the fundamental mode. Note that even though the equivalent fiber has a high NA (up to 0.37; see Fig. 3), the dispersion curves are essentially the same (to $10^{-3} - 10^{-4}$) whether they are calculated for the LP modes or for the true hybrid modes of the fiber. The quantitative differences between the curves of Fig. 9 are not due to limitations of the LPMA but to fundamental physical differences in the guiding mechanisms of solid-core and air-core fibers. It is, nevertheless, remarkable that in spite of these differences, the curves turn out to have such similar trends.

VII. Fundamental Mode Profile and Radius

The shape and radius of the fundamental mode are other parameters of interest. As an example, we plot in Fig. 10 the radial intensity profile of the fundamental mode computed for a core radius $R = 0.9\Lambda$ at a normalized frequency of 1.6156. Since the 2-D profile is not azimuthally symmetric, both the x and y cuts are shown. Each figure also shows the profile of the LP_{01} mode of the equivalent conventional fiber at that frequency. Except for the small side lobes of the HE_{11} modes, the actual and approximate profiles are close to each other. This comparison demonstrates that the LPMA model can also give a good qualitative description of the intensity profile of the fundamental modes of an air-core PBF, especially the dependence of the main lobe on the structural parameters. Because the LPMA model approximates the air-core fiber modes as LP modes, it clearly cannot predict the presence of side lobes. When the true mode field of the fiber has side lobes of substantial magnitude, the LPMA is, therefore, going to be somewhat off in its prediction of the fiber mode radius.

To determine the range of validity of this agreement, we calculated the radius W_0 of the fundamental mode of a PBF and compared it to the LP_{01} mode radius of its equivalent conventional fiber for a wide range of frequencies and core radii. In both the exact and the LPMA simulations, the mode effective area A_{eff} was calculated by integrating the intensity

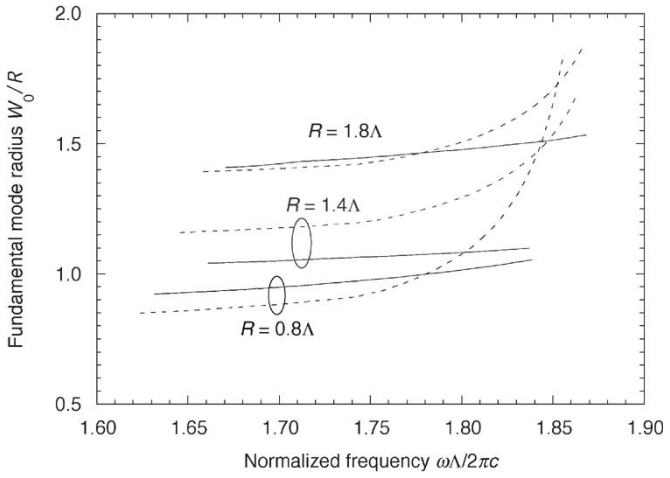

Fig. 11. Frequency dependence of the fundamental mode radius for selected core radii, calculated exactly (solid curves) and with the LPMA model (dashed curves).

profile $I(x, y)$ numerically using the expression of A_{eff} for a first-order process

$$A_{\text{eff}} = \frac{1}{I(0,0)} \int_0^\infty \int_0^\infty I(x,y)dxdy \tag{10}$$

and defining the mode radius W_0 using $A_{\text{eff}} = \pi W_0^2/2$. The dependence of the normalized mode radius W_0/Λ on frequency is plotted in Fig. 11 for the HE_{11} mode for three values of the air-core radius (solid curves) and for the LP_{01} mode radius of the corresponding equivalent conventional fiber (dotted curves). Again, the accuracy is fairly good for large cores but rather poor in the single-mode range. However, there are several striking similarities between the two fibers. At lower frequencies (below ~ 1.8), which is most of the mode's existence range, the radii of both modes depend weakly on frequency and are reasonably close. The main discrepancy occurs at higher frequency (above ~ 1.8), where the radius of the HE_{11} mode does not increase nearly as much as in a conventional fiber. The HE_{11} mode radius is a weak function of frequency, and, thus, a weak function of NA. For example, for $R = 0.8\Lambda$, as the frequency is increased from ~ 1.63 (low cutoff) to ~ 1.84 (high cutoff), W_0/Λ varies from ~ 0.92 to ~ 1.05 (see Fig. 11), although over this frequency range, NA varies from ~ 0.31 to ~ 0.16 (see Fig. 3).

This interesting behavior is a direct consequence of guiding light with a photonic-crystal cladding. First, because of the large index difference between the core $(n_1 = 1)$ and the medium surrounding it (here silica, index of ~ 1.45), the electric field of the fundamental mode at the air–solid boundary of the core is small (see Fig. 10), and, consequently, the shape of the mode's central lobe changes little with frequency. Second, because light is guided by multiple reflections in a photonic crystal, a small change in the field penetrating the cladding results in a sizable change in the mode phase velocity. Stated differently, the mode effective index is a strong function of the (small) fractional energy in the cladding. For example, simulations show that for $R = 0.8\Lambda$, when the frequency is increased from 1.62 to 1.84 (a change in NA from ~ 0.31 to 0.157), the fractional energy in the cladding increases from 22.1% to 30.2% only (the same NA change in a conventional fiber would change this fractional energy from $\sim 7.7\%$ to $\sim 27\%$). This is the basic reason why the mode intensity profile does not change significantly when the frequency approaches ω_U, even though NA approaches zero: The mode is forced to change shape, but only minimally. As a result of these two combined properties, at all frequencies, most of the mode energy is confined in the central lobe, and since the shape of this lobe depends weakly on frequency, the mode radius also depends weakly on frequency, as predicted by the exact model in Fig. 11.

These results enable us to predict simply the divergence angle θ_d of the HE_{11} mode of a PBF. The $1/e$ divergence half-angle is related to the mode radius W_0 by

$$\theta_d \approx \frac{\lambda}{\pi W_0}. \tag{11}$$

The divergence angle of the HE_{11} mode is, thus, also a weak function of frequency.

VIII. Bending Loss

The analogy between solid-core and air-core fibers can also be used to provide a qualitative interpretation for the so-far unexplained bending-loss behavior of air-core fibers. Hansen *et al.* [14] have shown experimentally that when an air-core fiber is subjected to a macrobend, the bend-induced loss is surprisingly weak, even for tight bends (4-mm radius). This loss was also found to be essentially independent of wavelength across most of the bandgap, except at the short-wavelength end of the bandgap, where the loss increases abruptly.

These three features are indeed well predicted by the definition of NA introduced in Section II. First, at long wavelengths (low frequencies), the NA of an air-core fiber (NA) is very large (~ 0.35; see Fig. 3), and the fiber loss is, therefore, expected to be quite tolerant to bending, as observed experimentally. Second, because the NA remains high up to fairly high frequencies (see Fig. 3), the bending loss is expected to remain low across most of the bandgap. For example, if we use, somewhat arbitrarily, an NA of 0.1 as representative of a standard conventional fiber, and, thus, of a standard tolerance to bending loss, then reference to Fig. 3 shows that the bending loss should remain very small up to a normalized frequency of ~ 1.88, i.e., over about 93% of the bandgap. This value compares quite well with the value of 92% calculated from [14, Fig. 6(b)]. Finally, for higher frequencies (above 1.88 in this example), the NA drops towards zero extremely quickly (see Fig. 3), which suggests that the bending loss should climb abruptly, again, as observed in actual fibers [14]. Note that NA, not NA', is the relevant parameter that controls the bending-loss behavior, because it describes the equivalent maximum angle of propagation of the modes in the fiber, and because it is only the high-angle portions of the mode's angular spectrum that suffer from bending-induced loss. The concept of NA introduced in this paper, therefore, provides a simple qualitative interpretation of the strength and wavelength dependence of macrobend loss in air-core fibers.

IX. Conclusion

From basic principles, we have shown that the core modes of an air-core PBF are expected to exhibit similar qualitative and quantitative behaviors as the LP modes of an equivalent conventional (solid core) fiber. The step-index profile of this equivalent fiber is a frequency-dependent quantity entirely determined by the longitudinal propagation constants k_z of the upper and lower bandgap edges of the PBF, which are straightforward to calculate on a standard computer. This analogy leads to the important definition of the effective NA of a PBF. We confirmed the validity of this equivalence by comparing the exact mode properties of a PBF to the properties of the LP modes of its equivalent conventional fiber and by showing that exact and approximate predictions match quite well. This description provides for the first time a simple intuitive means of explaining qualitatively the mode behavior of PBFs, including dispersion, mode size, and bending loss. It also constitutes a fast and simple tool to model approximately, using a simple LP-mode simulator, the main characteristics of the core modes of a PBF, including the number of modes, their cutoffs, effective index, and dispersion, and the dependence of these quantities on the core size and the photonic-crystal geometry and air-filling ratio.

Acknowledgment

The authors are thankful to V. Dangui for helpful discussions and help with the modeling of LP modes.

References

[1] T. P. White, R. C. McPhedran, L. C. Botten, G. H. Smith, and C. Martijn de Sterke, "Calculations of air-guided modes in photonic crystal fibers using the multipole method," *Opt. Express*, vol. 9, no. 13, pp. 721–732, Nov. 2001.

[2] J. Broeng, S. Barkou, T. Sondergaard, and A. Bjarklev, "Analysis of air-guiding photonic bandgap fibers," *Opt. Lett.*, vol. 25, no. 2, pp. 96–98, Jan. 2000.

[3] K. Saito, N. A. Mortensen, and M. Koshiba, "Air-core photonic band-gap fibers: The impact of surface modes," *Opt. Express*, vol. 12, no. 3, pp. 394–400, Feb. 2004. [Online]. Available: http://www.opticsexpress.org/abstract.cfm?URI=OPEX-12-3-394

[4] D. C. Allan, N. F. Borrelli, M. T. Gallagher, D. Müller, C. M. Smith, N. Venkataraman, J. A. West, P. Zhang, and K. W. Koch, "Surface modes and loss in air-core photonic band-gap fibers," in *Proc. SPIE*, A. Adibi, A. Scherer, and S. Y. Lin, Eds, 2003, vol. 5000, Photonic Crystals Materials and Devices, pp. 161–174.

[5] H. K. Kim, J. Shin, S. Fan, M. J. F. Digonnet, and G. S. Kino, "Designing air-core photonic-bandgap fibers free of surface modes," *IEEE J. Quantum Electron.*, vol. 40, no. 5, pp. 551–556, May 2004.

[6] V. Dangui, M. J. F. Digonnet, and G. S. Kino, "A fast and accurate numerical tool to model the modal properties of photonic-bandgap fibers," *Opt. Express.* , submitted for publication.

[7] N. A. Mortensen, J. R. Folken, P. M. W. Skovgaard, and J. Broeng, "Numerical aperture of single-mode photonic crystal fibers," *IEEE Photon. Technol. Lett.*, vol. 14, no. 8, pp. 1094–1096, Aug. 2002.

[8] S. G. Johnson and J. D. Joannopoulos, "Block-iterative frequency-domain methods for Maxwell's equations in planewave basis," *Opt. Express*, vol. 8, no. 3, pp. 173–190, Jan. 2001.

[9] J. D. Joannopoulos, R. D. Meade, and J. N. Winn, *Photonic Crystal: Molding the Flow of Light*. Princeton, NJ: Princeton Univ. Press, 1995, p. 96.

[10] H. K. Kim, M. J. F. Digonnet, J. Shin, S. Fan, and G. S. Kino, "Nomenclature and properties of the modes of air-core photonic-bandgap fibers," submitted for publication.

[11] A. W. Snyder and J. D. Love, *Optical Waveguide Theory*. London, U.K.: Chapman & Hall, 1983, p. 320.

[12] D. Gloge, "Weakly guiding fibers," *Appl. Opt.*, vol. 10, no. 10, pp. 2252–2258, Oct. 1971.

[13] R. F. Cregan, B. J. Mangan, J. C. Knight, T. A. Birks, P. S. J. Russell, P. J. Roberts, and D. A. Allan, "Single-mode photonic band gap guidance of light in air," *Science*, vol. 285, no. 5433, pp. 1537–1539, Sep. 1999.

[14] T. P. Hansen *et al.*, "Air-guiding photonic bandgap fibers: Spectral properties, macrobending loss, and practical handling," *J. Lightw. Technol.*, vol. 22, no. 1, pp. 11–15, Jan. 2004.

Michel J. F. Digonnet received the degree of engineering from the Ecole Supérieure de Physique et de Chimie de la Ville de Paris, Paris, France, and the Diplome d'Etudes Approfondies in coherent optics from the University of Paris, Orsay, France, in 1978, and the M.S. and Ph.D. degrees from the Applied Physics Department, Stanford University, Stanford, CA, in 1980 and 1983, respectively. His doctoral research centered on wavelength division multiplexing (WDM) fiber couplers and single-crystal fiber lasers and amplifiers.

From 1983 to 1986, he was employed by Litton Guidance and Control, Chatsworth, CA, as a Visiting Scholar at Stanford, conducting research in miniature solid-state sources and integrated optics for fiber sensors. From 1986 to 1990, he was involved in the development of dye and 2-μm solid-state lasers, fiber sensors, and delivery systems for laser angioplasty at MCM Laboratories, Mountain View, CA. Since then, he has been a Senior Research Associate in Stanford University's Applied Physics Department. His current interests include photonic-bandgap fibers, fiber sensors and sensor arrays, high-power ceramic and fiber lasers and amplifiers, fiber gratings, optical microcavities, and poled glasses. He has published 175 articles, issued 55 patents, edited several books, taught courses in fiber amplifiers, lasers, and sensors, and chaired numerous conferences on optical fiber devices and fiber sensors.

Hyang Kyun Kim (M'03–A'04–M'04) received the B.S. degree in physics from Yonsei University, Seoul, South Korea, in 1987, and the M.S. and Ph.D. degrees in physics from the Korea Advanced Institute of Science and Technology (KAIST), Taejon, South Korea, in 1990 and 1994, respectively.

She was a Senior Research Engineer at the Electronics and Telecommunication Research Institute (ETRI), Taejon, from 1994 to 1999, a Member of Technical Staff, Bell Labs, Lucent Technologies, NJ, from 1999 to 2000, and a Principal Staff Engineer, Novera Optics, CA, from 2001 to 2002. Since 2002, she has been at the E. L. Ginzton Laboratory, Stanford University, Stanford, CA, as a Research Associate. Her research interests include various aspects in fiber optic communication systems and optical fiber sensors. She is currently working on photonic-crystal fibers and designing, characterization, and applications for sensors/communication systems and fiber optic components.

Gordon S. Kino received the B.Sc. and M.Sc. degrees in applied mathematics from London University, London, U.K., in 1948 and 1950, respectively, and the Ph.D. degree in electrical engineering from Stanford University, Stanford, CA, in 1955.

He is a W. M. Keck Foundation Professor of Electrical Engineering, Emeritus, and Courtesy Professor of Applied Physics, Emeritus. He has published more than 400 papers and graduated more than 70 doctoral students.

Prof. Kino is a member of the National Academy of Engineering and a Fellow of APS and AAAS.

Shanhui Fan was born in 1972. He was an undergraduate student in physics at the University of Science and Technology of China, Hefei, Anhui, China, from 1988 to 1992, and he received the Ph.D. degree in physics from the Massachusetts Institute of Technology (MIT), Cambridge, in 1997.

He was a Postdoctoral Research Associate in Physics at MIT from 1997 to 1999 and a Research Scientist at the Research Laboratory of Electronics, MIT, from 1999 to 2001. He has been an Assistant Professor at the Department of Electrical Engineering, Stanford University, Stanford, CA, since 2001. His interests include theory and simulations of photonic and solid-state materials and devices, photonic crystals, nanoscale photonic devices and plasmonics, quantum optics, computational electromagnetics, and parallel scientific computing.